Colloids and Surfaces B: Biointerfaces 159 (2017) 696–704

Contents lists available at ScienceDirect

Colloids and Surfaces B: Biointerfaces

journal homepage: www.elsevier.com/locate/colsurfb

Modification of hysteresis behaviors of protein monolayer and the corresponding structures with the variation of protein surface charges

Bijay K. Sah, Sarathi Kundu*

Soft Nano Laboratory, Physical Sciences Division, Institute of Advanced Study in Science and Technology, Vigyan Path, Paschim Boragaon, Garchuk, Guwahati, Assam 781035, India

ARTICLE INFO

Article history:
Received 16 June 2017
Received in revised form 9 August 2017
Accepted 17 August 2017
Available online 24 August 2017

Keywords:
BSA monolayer
Compression-decompression
Hysteresis
Out-of-plane structures
Structural modification

ABSTRACT

Successive compression-decompression cycles of the surface pressure (π) – specific molecular area (A) isotherms of protein (BSA) monolayers show that reversible hysteresis persists if the protein molecules contain effective positive or negative surface charges. However, for neutral condition, i.e., close to the isoelectric point of the protein, irreversibility in the hysteresis behaviour dominates. Out-of-plane structures obtained from the X-ray reflectivity analysis suggest that at lower surface pressure monomolecular layer of BSA is formed on the water surface. With increasing surface pressure, molecules start to lift-up from the water surface in such a way that semi-major axis makes an angle with the water surface. Depending on the surface pressure and surface charge of BSA, monomolecular or bimolecular layer of tilted BSA molecules is formed on the water surface, however, formation of bimolecular layer is observed when the pH is relatively closer to the BSA isoelectric point. After complete decompression, tilted monomolecular or bimolecular structures again transform into monomolecular layer as evidenced from the structural analysis of the films deposited at lower surface pressures in the second compression, however, structural hysteresis varies depending upon the subphase pH or protein surface charge. Structures obtained from the films deposited at first and second compressions at lower pressure implies that although structural dissimilarity is present but structural hysteresis is only present near the isoelectric point of BSA and becomes negligible below and above that pH. Competitive electrostatic and van der Waals interactions are responsible for such hysteresis behaviours and structural modifications.

1. Introduction

Proteins are one of the most important biomolecules that play multitude roles in living beings. Their behaviors and responses can be controlled by regulating the environmental conditions such as pH, the presence of additives, ionic strength, etc. Proteins, especially blood and plasma proteins, are the major target of various viruses [1], medicines [2], metal ions [3,4], artificial drugs [5], etc. The functions of proteins are strongly related to their structures which again depend upon the microenvironment around their reaction centers [6,7] that are responsible for both the specific and non-specific interactions among the protein residues.

Proteins play a crucial role as emulsion stabilizers in the food industry and have many other practical applications. Studies on protein adsorption on different interfaces have gained widespread interest due to their large biomedical and industrial applications like manufacturing of medical devices, food processing, drug delivery, etc. For example, the interaction of artificial solid surfaces (like kidney implants, heart valves or contact lenses) with surrounding fluid results in protein adsorption which has a great influence on subsequent interfacial events, like blood coagulation or surface interaction with cells and tissues. Proteins have also been used extensively for biosensor applications and chromatographic purification of various drugs, peptides and antibodies [8–14]. Globular proteins even after being water soluble can adsorb at the air-water interface forming dense monolayers. Protein films at the air-water interface can be formed either by spreading the protein solution on water surface [15] or by specific adsorption of the protein molecules which are injected into the aqueous subphase [16,17]. There are numerous methods to immobilize biomaterials like proteins on the solid surfaces like self-assembly, sol-gel process, drop casting, Langmuir-Blodgett (LB) technique, etc [18–23]. Among all the above mentioned techniques the LB technique is one of the most widely used technique as it can build ordered and closed packed structures on the interested substrates [24–27] and the film thickness can be tuned at the molecular level, for instances

* Corresponding author.
E-mail address: sarathi.kundu@gmail.com (S. Kundu).

http://dx.doi.org/10.1016/j.colsurfb.2017.08.032
0927-7765/

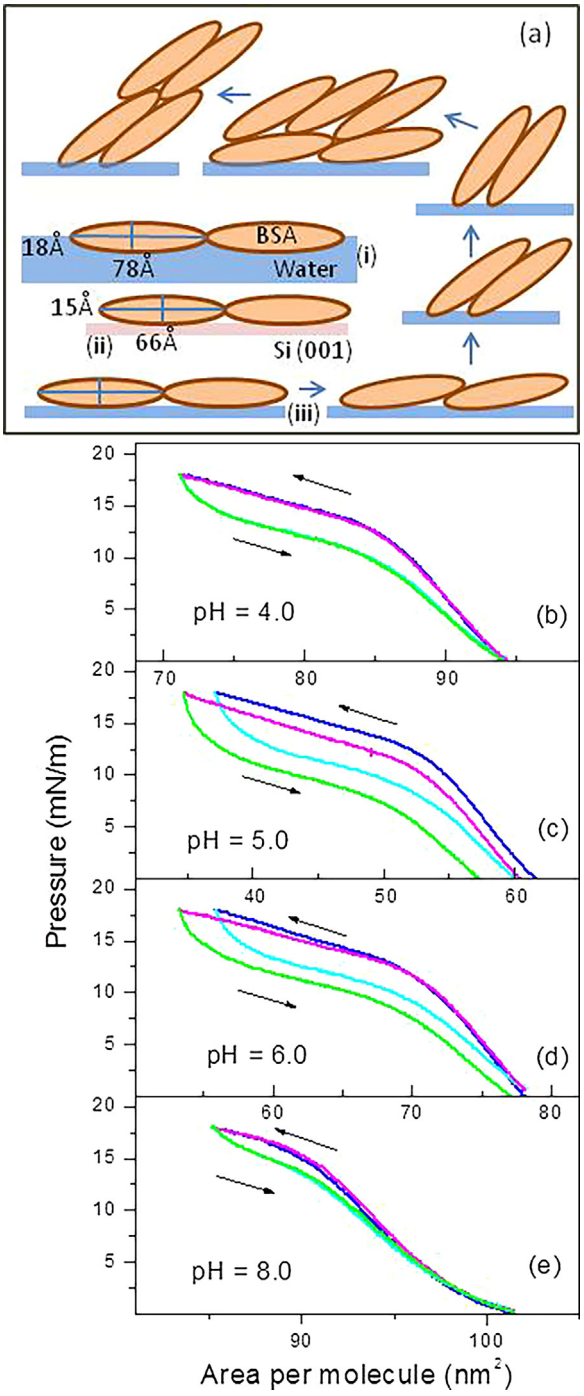

Fig. 1. (a) Schematic representation of molecular dimensions of BSA molecule on (i) water, (ii) solid surfaces and (iii) structural modifications of BSA molecules with increasing barrier compression or surface pressure. First and second compression–decompression surface pressure (π)–specific molecular area (A) isotherm cycles of protein (BSA) monolayer at four different subphase pH values, i.e., at pH ≈ 4.0 (b), 5.0 (c), 6.0 (d) and 8.0 (e). Maximum errors in area and pressure measurements are of ≈±0.01 nm^2/molecule and ±0.005 mN/m respectively.

ultrathin films of penicillin G acylase [28], heparin [29,30], etc. In addition to spectroscopic methods, X-ray and neutron scattering techniques are also used to explore the structures of different proteins adsorbed on different solid surfaces [31,32]. Despite of the surface induced modifications, proteins in their transferred films preserve their secondary and tertiary structures, as shown by the circular dichroism spectra and specific immunoglobulin's reaction centers [33].

Among all the proteins, Bovine Serum Albumin (BSA) has been studied intensively as it is an ideal protein for physical, chemical and biological studies. BSA is a globular protein and initially it was modeled as a prolate ellipsoid [34] of dimensions ≈ 70 Å × 20 Å × 20 Å, later on it was considered as an oblate ellipsoid of dimensions ≈ 12.5 Å × 42 Å × 42 Å [35]. However, an oblate form of dimensions ≈ 9 Å × 39 Å × 39 Å was also considered at pH ≈ 7.0 to explain neutron scattering results [36]. Probably the size depends upon the specificity of the BSA molecules, experimental conditions and measuring techniques. The isoelectric point (pI) of BSA is ≈ 4.8 and contains three main domains held together by the disulfide bonds. The net charge in each domain is different and pH dependent, thus, pH can alter the surface charge of the BSA molecule. Above the pI, protein possesses net negative surface charge whereas below the pI net positive surface charge exists and at the pI, it remains neutral. It has also been evidenced that pH-dependent conformational changes, i.e., folded to unfolded transition mainly occurs below pH ≈ 4.0 [36,37] and BSA keeps its structure unaltered from pH ≈ 4.0 to ≈ 9.0 within the concentrations of 10–50 mg/ml [36].

It is a well-established fact that globular proteins form a monolayer at the air-water interface but their structural modifications in molecular level with successive compression-decompression cycles at different surface charge states are not explored properly. The reversible/irreversible behaviors of protein layers with mechanical compression and expansion cycles may mimic different physiological phenomena. In general, the response of the film under compression and expansion holds the key to determining the stability of numerous colloidal systems such as emulsions and foams [38]. Moreover, structural reversibility has been observed in the tendons of forearms of animals [39] and in the trans-membrane proton pumping mechanism of the purple membrane (bacteriorhodopsin) [40,41]. Reversible structural changes of molecular crystals and polymers have also been reported [42,43]. Like organic systems, amorphous-to-crystalline reversible phase transformations in inorganic materials like GaSb [44] and reversible martensitic transitions in some shape-memory alloys are also observed [45] which may have potential applications. However, reversible/irreversible behaviors of proteins are not properly explored with the variation of the surface charges of the proteins.

In this article, we have investigated the reversible/irreversible behaviours of BSA monolayer with the successive compression-decompression cycles of the surface pressure (π) – specific molecular area (A) isotherms for different surface charge states of BSA molecules around its isoelectric point at the air-water interface and the corresponding structural modifications at the molecular level are identified. The surface charge of BSA was modified by changing the water subphase pH. Brewster angle microscopy (BAM) was used to obtain the film pattern on the water surface at different surface pressures of the monolayer for a particular subphase pH. Out-of-plane structures and in-plane morphologies of the protein films at the different conditions of the π-A isotherms are obtained from X-ray reflectivity (XRR) and atomic force microscopy (AFM) after depositing the protein films on the hydrophilic silicon surfaces. Modification of the isotherm nature with the variation of water pH or protein surface charges, hysteresis behaviors of the protein layer and the corresponding structures and patterns are explored.

2. Experimental

Bovine Serum Albumin (BSA) (catalog No. A2153) was purchased from Sigma-Aldrich and used without further purification. BSA stock solution of 1 mg/ml was prepared by dissolving required

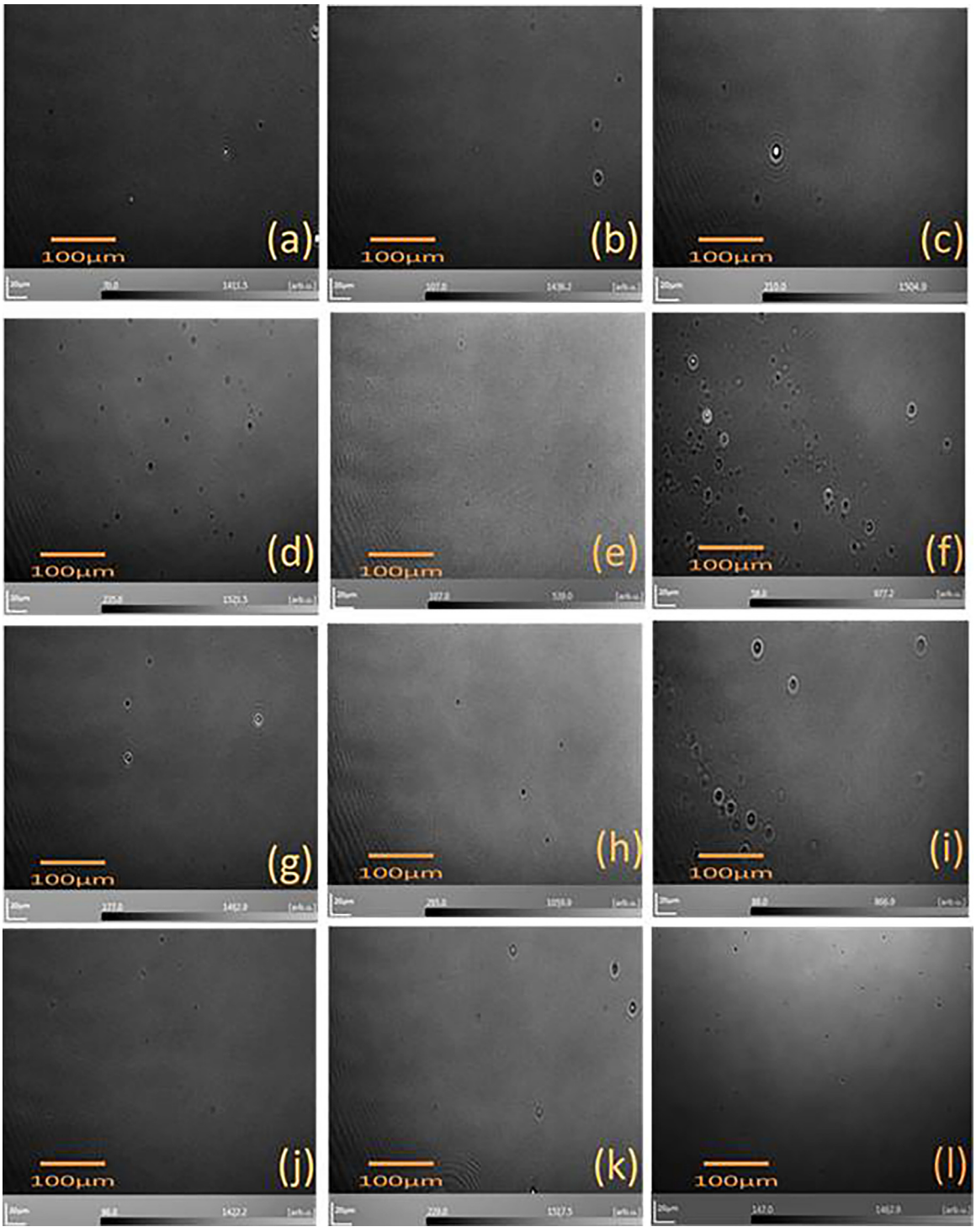

Fig. 2. Typical BAM images of BSA monolayers during first compression at lower ($\pi = 5$ mN/m) and higher ($\pi = 19$ mN/m) surface pressures are shown in first and second column, while third column is for the same film at lower ($\pi = 5$ mN/m) pressure during second compression at four different pH values i.e. ≈ 4.0 (a, b and c), 5.0 (d, e and f), 6.0 (g, h and i) and 8.0 (j, k and l). The bars represent 100 μm and spatial resolution is of ≈2 μm.

amount of BSA in Milli-Q water (resistivity 18.2 MΩ.cm) before each experiment. The specific volume of BSA solution was carefully spread with the help of syringe on the surface of water subphase contained in a double-barrier Langmuir trough made of Teflon (Apex Instruments). Any changes in the surface tension were well recorded through a paper Wilhelmy plate. Before compression, the system was allowed to attain some equilibrium. Monolayers were compressed and expanded at a constant speed of 5 mm/min during isotherm measurements and film depositions. Just before deposition of the films at different surface pressures, the monolayer was allowed to gain stability for a time lapse of about 10 min. Depositions were carried out at a speed of 2 mm/min. Prior to the deposition, Si (001) substrates were properly cleaned after keeping in a mixed solution of ammonium hydroxide (NH_4OH, Merck, 30%), hydrogen peroxide (H_2O_2, Merck, 30%), and Milli-Q water (H_2O: NH_4OH: H_2O_2 = 2:1:1, by volume) for 5–10 min at 100°C. Immediately after cleaning, all the substrates were kept inside the Milli-Q water until LB deposition. Such cleaned hydrophilic silicon sur-

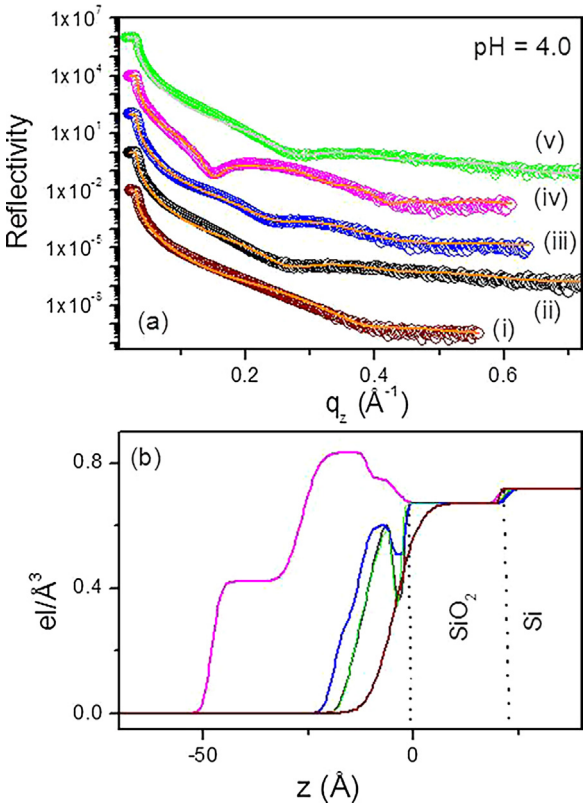

Fig. 3. (a) X-ray reflectivity data (circle) and the corresponding fitted curves (solid line) obtained from the (i) bare silicon and BSA films deposited at (ii) 5 mN/m, (iii) 15 mN/m and (iv) 19 mN/m during first compression, and again at (v) 5 mN/m during second compression of the BSA monolayer at pH ≈ 4.0. (b) Corresponding electron density profiles extracted from the fitting of the reflectivity data. Maximum errors in electron density (ρ) and thickness (z) are of 5–7% and 3–5% respectively.

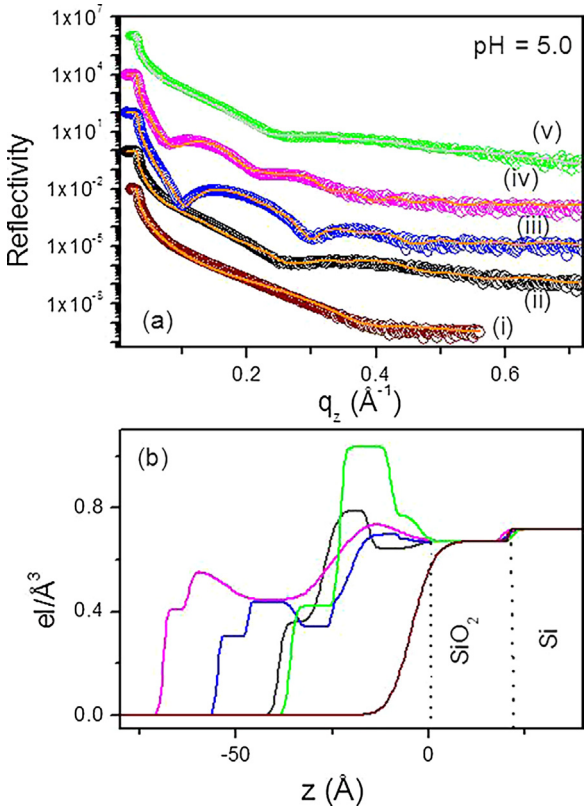

Fig. 4. (a) X-ray reflectivity data (circle) and the corresponding fitted curves (solid line) obtained from the (i) bare silicon and BSA films deposited at (ii) 5 mN/m, (iii) 15 mN/m and (iv) 19 mN/m during first compression, and again at (v) 5 mN/m during second compression of the BSA monolayer at pH ≈ 5.0. (b) Corresponding electron density profiles extracted from the fitting of the reflectivity data. Maximum error in electron density (ρ) and thickness (z) is of 5–7% and 3–5% respectively.

face makes 15°–18° contact angle with the water drop. All surface pressure (π) – specific molecular area (A) isotherm measurements and film depositions were performed at an ambient temperature of 23°C (±1°C). The pH of the water subphase was maintained at ≈4.0, 5.0, 6.0 and 8.0 for different experimental conditions. The main motivation was to see the isotherm behaviors and structures around the isoelectric point of BSA.

Visualizations of domain patterns of BSA thin films at different subphase pH and surface pressures were performed by means of Brewster angle microscopy (BAM) using a nanofilm_EP4 BAM. The instrument consists of a standard 50 mW solid state laser, emitting p-polarized light at a wavelength of 658 nm by using a polarizer. The reflected light coming from the water or BSA film surfaces are imaged to a computer controlled high-quality CCD camera which is attached to a real time frame grabber with 1392 × 1040 pixels through a 10× magnification objective, yielding a spatial resolution of ≈2 μm. A black wedge-shaped glass plate is placed at the bottom of the trough to reflect any light transmitted through the subphase out of the optical axis and to minimize the convection in the trough.

Surface topography of all the deposited films of BSA at different subphase pH was studied through an atomic force microscope (NTEGRA Prima, NT-MDT Technology). All the scans were undertaken in semi-contact mode using silicon cantilever having spring constant of ≈11.8 N/m [46]. For all the deposited films scans were carried out in a constant force mode over several portions of the film with scan area of 5 μm × 5 μm. WSxM software [47] was used for AFM image processing and analysis.

X-ray reflectivity (XRR) measurements of BSA thin films were carried out using an X-ray diffractometer (XRD) setup. Diffractometer (D8 Advanced, Bruker AXS) has a copper (Cu) source in a sealed tube followed by a Göbel mirror for the selection and enhancement of the CuK$_\alpha$ radiation (=1.54 Å). NaI scintillation (point) detector was used for detecting the scattered beam. Data were taken in specular condition, i.e., the incident angle (θ) was kept equal to the reflected angle (θ) such that both lie in the same scattering plane. Under such condition, a non-vanishing wave-vector component, q_z, is given by $(4\pi/\lambda)\sin\theta$. Analysis of XRR data was pursued using Parratt's formalism [48] where the film is supposed to be a stack of multiple homogeneous layers with sharp interfaces. However, to analyse the XRR data, surface and interfacial roughness's have been included [49,50]. XRR data effectively provides electron-density variation, i.e., the electron-density profile (EDP) [49,51] which is in-plane (x–y) average electron density (ρ) as a function of depth (z) with high resolution [49–53]. From the EDPs out-of-plane structures of the deposited films can be obtained.

In the Parratt's formalism the reflectivity as a function of q_z for a thin film of thickness d over a substrate, is given as $R(q_z) = rr^*$, where

$$r_0 = \frac{r_{1,2} + r_{2,3}}{1 + r_{1,2}r_{2,3}}, \tag{1}$$

with r_{12} and r_{23} being the reflectance for the vacuum-film and film-substrate interfaces, respectively. The above calculation can be extended for n such thin stratified layers of thickness d and one arrives at a recursive formula in terms of Fresnel reflectance given by

$$r^F_{n-1,n} = \frac{r_{n,n+1} + F_{n-1,n}}{1 + r_{n,n+1}F_{n-1,n}} \exp(-iq_{n-1,n}d_{n-1}), \tag{2}$$

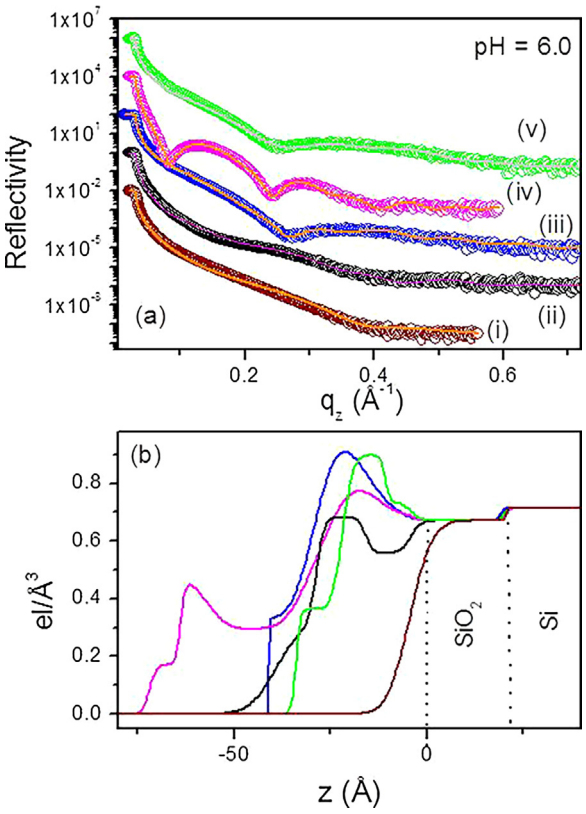

Fig. 5. (a) X-ray reflectivity data (circle) and the corresponding fitted curves (solid line) obtained from the (i) bare silicon and BSA films deposited at (ii) 5 mN/m, (iii) 15 mN/m and (iv) 19 mN/m during first compression, and again at (v) 5 mN/m during second compression of the BSA monolayer at pH ≈ 6.0. (b) Corresponding electron density profiles extracted from the fitting of the reflectivity data. Maximum error in electron density (ρ) and thickness (z) is of 5–7% and 3–5% respectively.

where,

$$F_{n-1,n} = \frac{q_{n-1,z} - q_{n,z}}{q_{n-1,z} + q_{n,z}}. \quad (3)$$

In the n^{th} stratified layer the corresponding wave vector is defined as $q_{n,z} = (q_z^2 - q_{n,c}^2)^{1/2}$. The Fresnel reflectance for the interface between n^{th} and $(n-1)^{\text{th}}$ stratified layer is modified to include the roughness σ_n of the n^{th} stratified layer and one can finally write the reflectance of a rough surface as

$$r_{n-1,n} = r^F_{n-1,n} \exp(-0.5 q_{n-1,z} q_{n,z} \sigma_n^2). \quad (4)$$

In general, the electron density variation in a specimen is determined by assuming a model and comparing the simulated profile with the experimental data. EDP is extracted from the fitting of the experimental XRR data. For data fitting, each film was divided into a number of layers including roughness at each interface. Silicon substrate density and the density of thin (≈24 Å) silicon oxide layer formed on the silicon surface were kept constant during data fitting. Density of BSA was varied but it was less than the maximum BSA density in dry condition. For the films deposited at lower and higher surface pressures, three and six layers were used for better fitting. An instrumental resolution in the form of a Gaussian function and a constant background were also included at the time of data analysis.

3. Results and discussion

Compression-decompression π-A isotherm cycles (two cycles) of BSA monolayer formed at the air-water interface are shown in Fig. 1 for four different subphase pH, i.e., below and above the isoelectric point of BSA (≈4.8), in addition with the schematic diagram for the structural modifications of the BSA molecules inside the film as shown in Fig. 1(a). Isotherm cycles below the isoelectric point, i.e., at pH ≈ 4.0 are shown in Fig. 1(b), whereas nearly at isoelectric point, i.e., at pH ≈ 5.0 and above the isoelectric points, i.e., at pH ≈ 6.0 and 8.0 are shown in Fig. 1(c)–(e) respectively. From the isotherms, it is clear that the surface pressure starts to increase at A ≈ 95 nm^2 for pH ≈ 4.0, however, for pH ≈ 6.0 and 8.0, π starts to increase at A ≈ 77 and 102 nm^2 respectively. Nearly at the isoelectric point, i.e., at pH ≈ 5.0, π starts to increase at A ≈ 62 nm^2. For each isotherm, a plateau-like feature is observed nearly at 13 mN/m, which is shifted towards higher value at 15 mN/m for pH ≈ 8.0. Such plateau-like feature suggests that a structural rearrangement process takes place around that point, i.e., significant amount of molecular tilting or monolayer to bimolecular layer formation may occurs as shown in Fig. 1(a) as a cartoon. Considering BSA as oblate ellipsoid of radii a × a × b ≈ 39 Å × 39 Å × 9 Å as shown in Fig. 1(a), the calculated A will be $\pi a^2 \approx 47.8$ nm^2. Actually, with barrier compression or increasing surface pressure BSA molecules come closer to each other and depending upon their surface charge and hydrophobicity, molecular packing starts to form on the water surface. However, with more compression or surface pressure, the semi-major axes of BSA molecules start to tilt after compact packing and become more tilted. After a certain surface pressure bimolecular layer structures may form as shown in Fig. 1(a) depending upon the experimental conditions. With decompression, the surface pressure starts to decrease and try to follow the compression path, however, certain hysteresis exists in the compression-decompression cycle depending upon the subphase pH or protein surface charge. From the isotherms it is clear that the hysteresis is maximum for pH ≈ 5.0. In the second compression-decompression cycle, BSA monolayer shows nearly the same nature as obtained from the first cycle, however, the hysteresis amount has slightly enhanced for pH ≈ 5.0 and 6.0. Hysteresis is again very less for pH ≈ 8.0.

Brewster angle microscopy (BAM) is used to explore the topographic information of the protein films under different experimental conditions at the air-water interface [54–57]. Large numbers of images were obtained from BAM but only selective images are displayed because the images are nearly similar. Fig. 2 shows the BAM images of BSA films at four different subphase pH and three different surface pressures for each pH condition. First and second columns of Fig. 2 implies the BAM images of BSA monolayers during the first compression at lower (π = 5 mN/m) and higher (π = 19 mN/m) surface pressures, while third column is for the same film at same lower (π = 5 mN/m) pressure during the second compression. Images for the second cycle were also obtained which seemed very much similar to those obtained in the first cycle so the data are not shown. From the images it is clear that pure protein tends to form homogeneous adsorbed film at the air-water interface without forming any specific domain patterns but the reflected laser intensity slightly increases uniformly as the film density and thickness increases. The combination of relatively dark and bright portions observed in the images (Fig. 2f and i) at lower pressure during the second compression implies the boundary of the layered structure.

To obtain the out-of-plane structures at different isotherm points, films were deposited on the hydrophilic Si (001) substrates in single up-stroke from the BSA film covered water surface. Transfer ratio (TR) values for all the deposited films were well in between 0.82–1.14. Slight lower and higher values than unity implies that not all molecules get transfer from water to solid surface or dissolution of protein molecules into the water subphase may also occur respectively. After deposition on the Si (001) substrate the size of the BSA molecule might have reduced slightly as shown in Fig. 1(a).

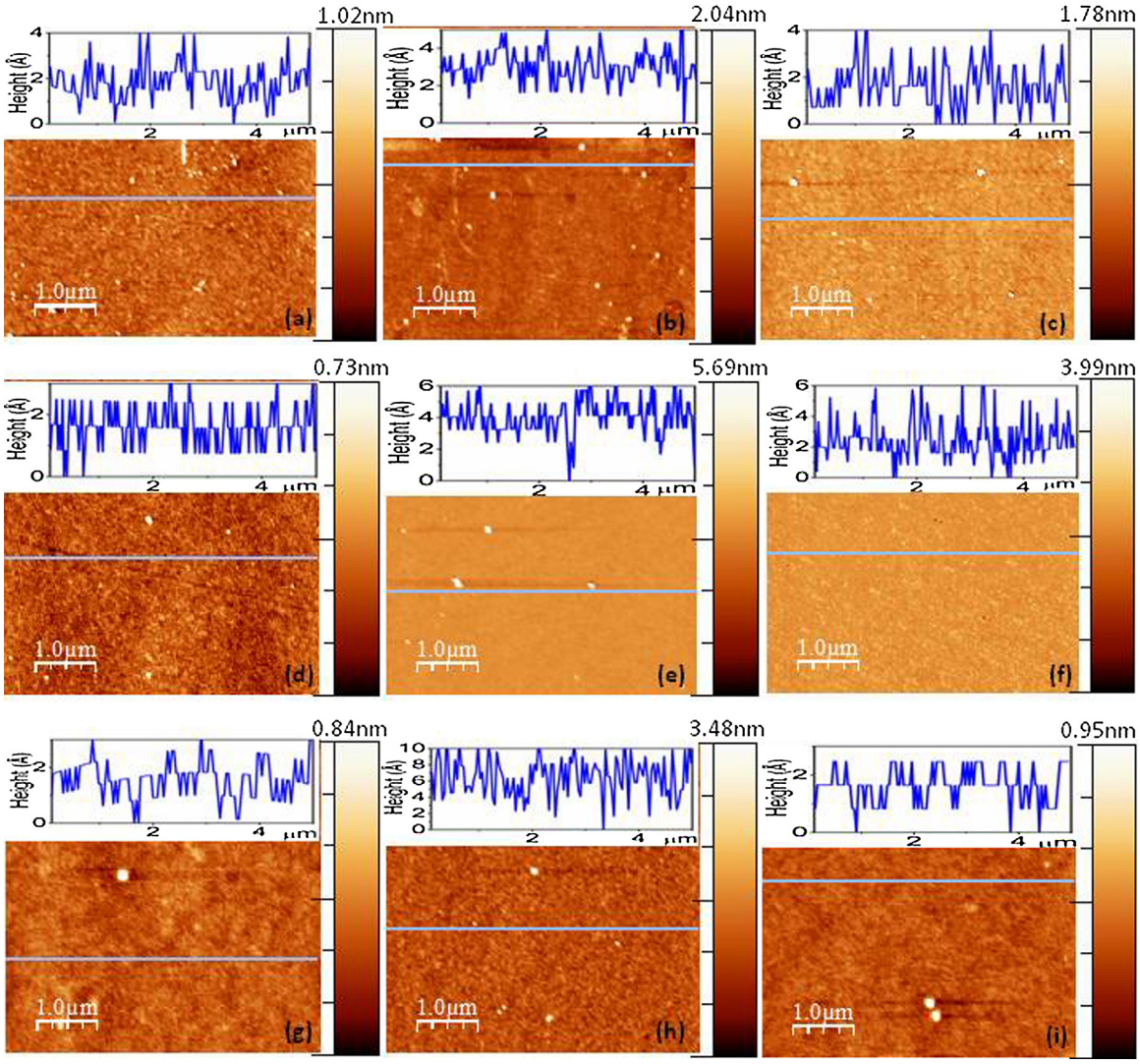

Fig. 6. AFM images of BSA films deposited on Si. First and second column are for the films deposited at lower ($\pi = 5$ mN/m) and higher ($\pi = 19$ mN/m) surface pressure during first compression, while third column is for the films deposited at lower pressure ($\pi = 5$ mN/m) during the second compression at three different pH values ≈ 4.0 (a–c), 5.0 (d–f) and 6.0 (g–i). Scan size: 5 μm x 5 μm. Insets are the corresponding line profiles. The bars represent 1.0 μm.

This slight volume reduction will increase electron density of the BSA molecules in dry condition. X-ray reflectivity data (open circles) and the corresponding fitted curves (solid lines) are shown in Figs. 3(a), 4(a) and 5(a) for the films deposited at subphase pH ≈ 4.0, 5.0 and 6.0 respectively. The corresponding EDPs obtained from the fitting are shown in Figs. 3(b), 4(b) and 5(b) respectively. From EDPs it is clear that monolayer of BSA are deposited at $\pi = 5$ mN/m for all the three pH and the semi-major axis is parallel to the Si (001) surface in case of pH ≈ 4.0 but for the other two pH values (i.e., for pH ≈ 5.0 and 6.0) the semi-major axis makes an angle of about ≈ 37° and 44° respectively. At $\pi = 15$ mN/m, film thickness slightly increases for pH ≈ 4.0 and 5.0 as obtained from the EDPs which implies that for pH ≈ 4.0 and 5.0 the tilting of the BSA molecules occurs as shown in Fig. 1(a) but in case of pH ≈ 5.0, in addition to that bimolecular layer formation takes place out of which in the lower molecular layer the semi-major axes of BSA are parallel with the Si (001) surface but in the upper molecular layer molecules are tilted by ≈ 31°. On the other hand for pH ≈ 6.0, EDP indicates that the film thickness remains constant but the film density increases implying that relatively less tilted molecules within the film gets tilted up to ≈ 44° and finally forms a denser layer. EDP obtained from the film deposited at $\pi = 19$ mN/m, suggest that maximum tilting of about ≈ 53° was obtained for BSA at the subphase pH ≈ 4.0 but for pH ≈ 5.0 and 6.0, the formation of the bimolecular layer was observed by the tilted BSA molecules.

For both the upper and lower molecular layer, BSA molecules are tilted by ≈ 36° with respect to the Si (001) surface. After full decompression when the film was deposited in the second compression at $\pi = 5$ mN/m, again monolayer structure was formed where the semi-major axes of BSA molecules were again seen to be parallel with the Si (001) surface as observed from the EDP. But the facts differ in case of the other two pH values (≈ 5.0 and 6.0) as the formation of monolayer structure is such that the BSA molecules are tilted by ≈ 36°. Thus, considering pH ≈ 4.0, it can be said that the reversibility obtained from the isotherm cycle is well maintained in the structural point of view also. For pH ≈ 6.0, although structural dissimilarity is present between the films deposited in first and second compression but nearly reversible hysteresis is observed from the first compression-decompression isotherm cycle and out-of-plane structures. However, irreversible hysteresis is confirmed from both the isotherm and structures of the BSA layer at pH ≈ 5.0 as structural reorganization takes place after the first isotherm cycle.

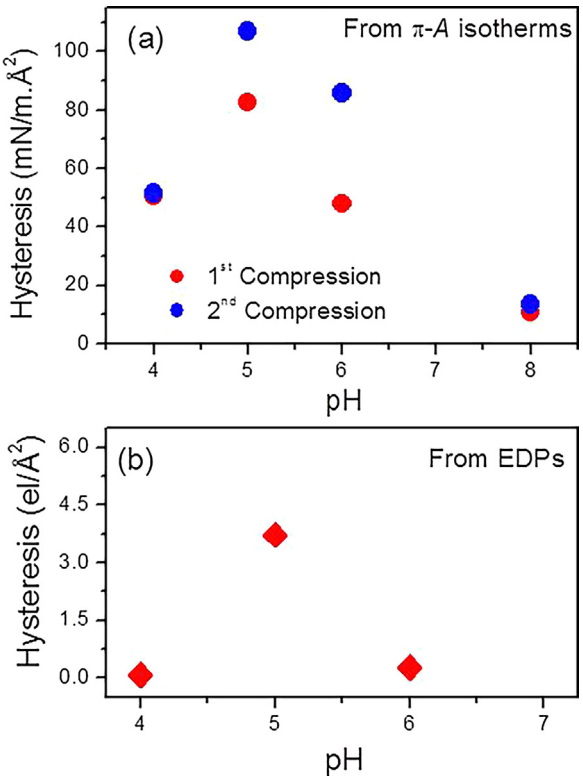

Fig. 7. Variations of (a) isotherm hysteresis with the subphase pH for the first and second cycles of the π-*A* isotherm and (b) structural hysteresis with solution pH obtained from the EDPs. Maximum error in hysteresis is of 2–7% respectively.

Similar isotherm nature observed at pH ≈ 4.0 and 8.0 implies that nearly the same reversible hysteresis and structural information will be obtained from the protein films at pH ≈ 8.0, like pH ≈ 4.0.

Surface morphology of the BSA films deposited on Si substrates at three different pH conditions (≈ 4.0, 5.0 and 6.0) around the BSA isoelectric point are characterized using AFM. AFM images depicting the surface topography of the BSA films are shown in Fig. 6, where films deposited at pH ≈ 4.0, 5.0 and 6.0 are shown in the first, second and third row respectively. Films deposited at lower (5 mN/m) and higher (19 mN/m) surface pressure during the first compression are shown in the left and middle column of Fig. 6, while films deposited at lower pressure (5 mN/m) during the second compression is shown in the right column. Irrespective of the pH conditions, BSA films show smooth morphology at lower and higher surface pressures and also after decompression at a lower pressure which is well in agreement with the BAM images. Line profiles are also shown in the insets of the corresponding figures of AFM to reveal the surface roughness information of the deposited films, which are ≈ 1.5 to 10.0 Å on average.

From the compression-decompression π-*A* isotherm cycles it is clear that the BSA monolayer shows complete reversible hysteresis at pH ≈ 4.0 and 8.0, and relatively very close to the reversible hysteresis at pH ≈ 6.0 as in the second cycle irreversibility is observed. However, irreversible hysteresis is prominent from the first cycle at pH ≈ 5.0. It is thus implied that when BSA is far from its pI value, i.e., contains net positive or negative surface charges the reversible hysteresis takes place. The variations of the isotherm hysteresis (both reversible and irreversible) with the subphase pH for the first and second cycles are shown in Fig. 7(a). In the reversible hysteresis the structural modification of BSA molecules in the monolayer during compression and decompression does not follow the same path and as a result hysteresis is observed, however, at the end of the decompression it adopts the same structure with which the first compression started. As during decompression, pressure was less than during compression so it means that during decompression more hydrophilic parts were exposed or some may have penetrated into the water subphase but again during second compression more hydrophobic parts were exposed to air side to have higher surface pressure. Although it has already been proved that within the pH range of 4.0–9.0 and concentration range of 10–50 mg/ml, BSA keeps its structure unaltered [34], however, due to the presence of surface charges below and above the isoelectric point, there is a possibility of slight desorption of BSA molecules towards water. Recent studies have also shown that proteins desorption can occur towards air [58,59] side also. Variations in compression-decompression isotherms are probably related to such structural modifications. For irreversible hysteresis where area per molecule has reduced after first decompression means that on average molecular reorganization has occurred and molecules are moved from the water surface towards air or water side, which can be obtained from the X-ray reflectivity analysis. From the integration of the EDPs obtained from the reflectivity analysis of the deposited films during first and second compressions it is clear that there is effectively no structural hysteresis at pH ≈ 4.0 and 6.0, although at pH ≈ 6.0 structural variation has occurred. However, integrated EDPs obtained from the films deposited at pH ≈ 5.0 implies that structural hysteresis is present at pH ≈ 5.0, i.e., near to the pI value of BSA. Variation of the structural hysteresis with solution pH is shown in Fig. 7(b).

The out-of-plane structural modifications for reversible and irreversible hysteresis are shown as a cartoon in Fig. 8. The figure implies that the BSA molecules remain as a monolayer at pH ≈ 4.0, only the semi-major axis of oblate shaped protein molecule changes from parallel to tilted conformation with increasing surface pressure and after decompression nearly the same structure is recovered towards lower pressure. However, at pH ≈ 5.0, molecules become tilted at the same pressure and the monolayer transforms into tilted bimolecular layer structure at higher surface pressure and then after decompression again monolayer structure is obtained but with net density modification. Although not shown in the cartoon but at pH ≈ 6.0, intermediate structural variation is there but on average tilted molecules in monolayer transform into tilted bimolecular layer and after decompression again monolayer of tilted molecules forms. From the hysteresis values obtained from the first cycles at different subphase pH and from the out-of-plane structures obtained from the EDPs, the energy for different structural transitions can be roughly estimated. The energy estimations were done from the hysteresis loop, i.e., from the difference between the compression and decompression isotherm which roughly gives the required energy for the structural modification. Thus, for changing from parallel to tilted configuration (tilt angle ≈ 53°) of BSA molecules, the amount of energy required is $\approx 50\text{–}52 \times 10^{-23}$ J and for changing from parallel/tilted monolayer configuration to tilted bimolecular layer configuration the amount of energy required is $\approx 83\text{–}95 \times 10^{-23}$ J. It is known that the protein surface has both local positive and negative surface charges. Depending upon the subphase pH, BSA takes net positive surface charge below the pI and net negative surface charge above the pI. Thus, due to the presence of such net positive/negative surface charges the electrostatic repulsion will be present which will help to repeal the molecules from each other during decompression to get the initial monolayer structure which was disturbed due to the external barrier compression. However, near pI, as BSA has no net surface charges so molecules will easily come closer to each other due to van der Waals attraction with external compression and will not feel any strong repulsion to form initial monolayer structure except local electrostatic interaction. Thus, it is a combination of electrostatic and van der Waals interactions which determines the final structure at a constant temperature depending upon the

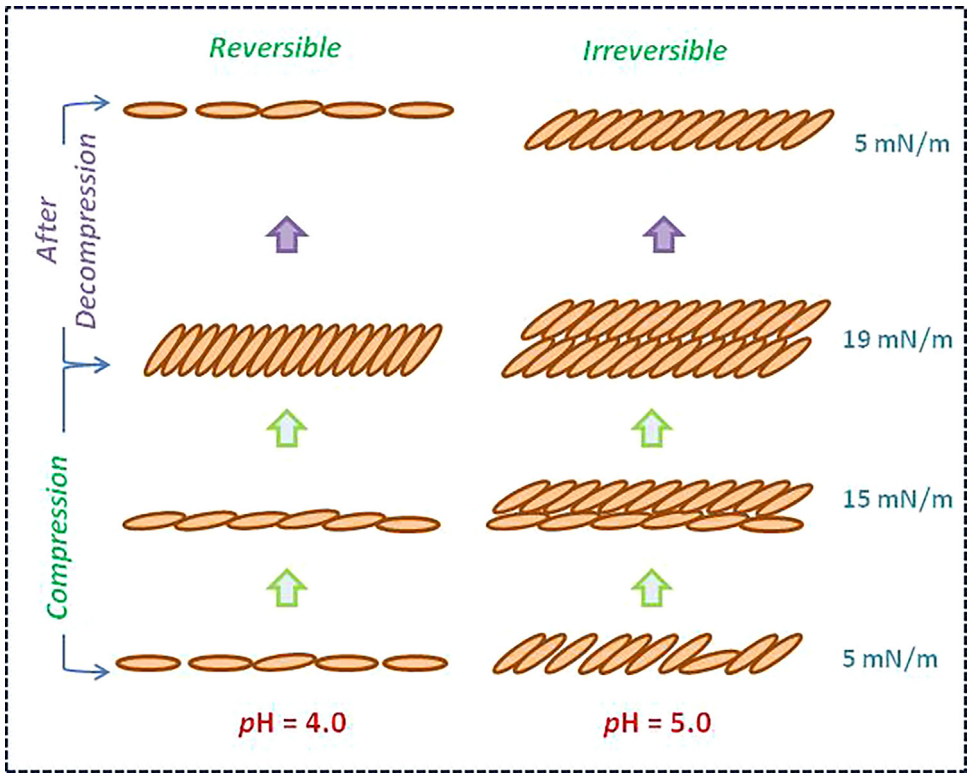

Fig. 8. Schematic representation of structural modifications for reversible and irreversible hysteresis at two different subphase pH, i.e., at pH ≈ 4.0 and 5.0. A monolayer of BSA gets a modification with increasing surface pressure during compression but after decompression structural hysteresis may or may not be present depending upon the subphase pH or BSA surface charge.

surface pressure and solution pH. Such type of reversible hysteresis exhibited by BSA molecules may mimic the role of lung protein during respiration.

4. Conclusions

Studies on reversibility behavior of Langmuir monolayer for serum albumin protein (BSA) at different subphase pH (≈4.0, 5.0, 6.0 and 8.0), both above and below the isoelectric point of BSA (≈4.8) has been carried out extensively. Protein molecules constituting the monolayer demonstrate reversible hysteresis in the presence of any net positive or negative surface charges at the molecular level compared to the irreversibility in the hysteresis due to the overall structural modifications when the net surface charge of the molecules remains nearly neutral. At lower pressure, the protein molecule remains parallel to the water surface but with the increasing surface pressure the parallel arrangement gradually gets distorted and with further increase in pressure, the molecule starts to rise maintaining some angular orientation depending on the net surface charge of the molecule. At sufficiently higher pressure, bi-molecular layer of tilted protein molecules are formed when the net surface charge on the molecules are very less or close to neutral. However, if the surface acquires some charge (positive/negative) it is observed that molecules are restricted only to a tilted monolayer. Moreover, once the conditionally oriented monolayer or bi-molecular structure is formed, the original state of the molecules can be achieved again for all pH values (except close to the pI value) by lowering the surface pressure to the initial value. Thus, this research work has shown that merely by varying the pH value we can categorically control and regulate upon the reversibility and irreversibility behaviors of protein layer.

Acknowledgement

The work is supported by Department of Science and Technology (DST), Nano Mission, India (Grant No. SR/NM/NS-1035/2013(G)).

References

[1] M.A. Calderwood, K. Venkatesan, L. Xing, M.R. Chase, A. Vazquez, A.M. Holthaus, A.E. Ewence, N. Li, T. Hirozane-Kishikawa, D.E. Hill, M. Vidal, E. Kieff, E. Johannsen, Proc. Natl. Acad. Sci. U. S. A. 104 (2007) 7606–7611.
[2] J.N. Tian, J.Q. Liu, J.Y. Zhang, Z.D. Hu, Chem. Pharm. Bull. 51 (2003) 579–582.
[3] L.Z. Wu, B.L. Ma, D.W. Zou, Z.X. Tie, J. Wang, W. Wang, J. Mol. Struct. 877 (2008) 44–49.
[4] B. Gong, Y. Chen, E.L. Christian, J.H. Chen, E. Chase, D.M. Chadalavada, R. Yajima, B.L. Golden, P.C. Bevilacqua, P.R. Carey, J. Am. Chem. Soc. 130 (2008) 9670.
[5] A. Taubert, Proc. Natl. Acad. Sci. U. S. A. 104 (2007) 20643–20644.
[6] H. Hegyi, M. Gerstein, J. Mol. Biol. 288 (1999) 147–164.
[7] N. Basdevant, H. Weinstein, M. Ceruso, J. Am. Chem. Soc. 128 (2006) 12766–12777.
[8] A. Girard-Egrot, P.S. Godoy, L. Blum, J. Adv. Colloid Interface Sci. 116 (2005) 205–225.
[9] F. Beigi, P. Lundahl, J. Chromatogr. A 852 (1999) 313–317.
[10] Y. Okahata, T. Tsuruta, K. Ijiro, K. Ariga, Langmuir 4 (1988) 1373–1375.
[11] J. Ramsden, J. Biosens. Bioelectron. 13 (1998) 593–598.
[12] S. Hou, J. Wang, C.R. Martin, Nano Lett. 5 (2005) 231–234.
[13] Z. Siwy, L. Trofin, P. Kohli, L.A. Baker, C. Trautmann, C.R. Martin, J. Am. Chem. Soc. 127 (2005) 5000–5001.
[14] C. Leger, P. Bertrand, Chem. Rev. 108 (2008) 2379–2438.
[15] A. Tronin, T. Dubrovsky, C. De Nitti, A. Gussoni, V. Erokhin, C. Nicolini, Thin Solid Films 238 (1994) 127–132.
[16] E.E. Uzgiris, R.D. Kornberg, Nature 301 (1983) 125–129.
[17] R. Kayushina, Y. Khurgin, G. Sukhorukov, T. Dubrovsky, Phys. B 98 (1994) 131–132.
[18] J.B. Lee, D. Kim, J. Choi, K. Koo, Colloids Surf. B: Biointerfaces 41 (2005) 163–168.
[19] T. Kamilya, P. Pal, G.B. Talapatra, J. Phys. Chem. B 111 (2007) 1199–1205.
[20] T. Kamilya, P. Pal, M. Mahato, G.B. Talapatra, J. Nanosci. Nanotechnol. 9 (2009) 2956–2964.

[21] T. Kamilya, P. Pal, M. Mahato, G.B. Talapatra, Mater. Sci. Eng. C 29 (2009) 1480–1485.
[22] K. Ariga, J.P. Hill, M.V. Lee, A. Vinu, R. Charvet, S. Acharya,Sci. Technol. Adv. Mater. 9 (2008), 014109.
[23] P. Pal, D. Nandi, T.N. Misra, Thin Solid Films 239 (1994) 138–143.
[24] X. Li, L. Zhang, X. Wang, I. Shimoyama, X. Sun, W.S. Seo, H. Dai, J. Am. Chem. Soc. 129 (2007) 4890–4891.
[25] G.G. Roberts, Langmuir Blodgett Films, Plenum, New York, 1990.
[26] D.K. Schwartz, Surf. Sci. Rep. 27 (1997) 245–334.
[27] J. Als-Nielsen, D. Jacquemain, K. Kjaer, F. Leveiller, M. Lahav, L. Leiserowitz, Phys. Rep. 246 (1994) 251–313.
[28] L. Pastorino, T.S. Berzina, V.I. Troitsky, M.P. Fontan, E. Bernasconi, C. Nicolini, Colloids Surf. B 23 (2002) 357–363.
[29] E.A. Aksoy, V. Hasirci, N. Hasirci, A. Motta, M. Fedel, C. Migliaresi, J. Bioact. Compat. Polym. 23 (2008) 505–519.
[30] D. Stoll, M.F. Templin, M. Schrenk, P.C. Traub, C.F. Vohringer, T.O. Joos, Front. Biosci. 7 (2002) 13–32.
[31] J.R. Lu, X. Zhao, M. Yaseen, Curr. Opin. Colloid Interface Sci. 12 (2007) 9–16.
[32] A.G. Richter, I. Kuzmenko, Langmuir 29 (2013) 5167–5180.
[33] P. Facci, V. Erokhin, C. Nicolini, Thin Solid Films 243 (1994) 403–406.
[34] L.R.S. Barbosa, F. Ortore, P. Spinozzi, S. Mariani, R. Bernstorff, J. Biophys. 8 (2010) 147–157.
[35] F. Zhang, F. Roosen-Runge, M.W.A. Skoda, R.M.J. Jacobs, M. Wolf, P. Callow, H. Frielinghaus, V. Pipich, S. Prévost, F. Schreiber, Phys. Chem. Chem. Phys. 14 (2012) 2483–2493.
[36] S. Kundu, K. Das, V.K. Aswal, Chem. Phys. Lett. 578 (2013) 115–119.
[37] T. Peters Jr., Adv. Prot. Chem. 37 (1985) 161–245.
[38] B.S. Murray, E. Dickinson, FoodSci. Technol. Int. 2 (1996) 131–145.
[39] J.H. Clark, Proc. Natl. Acad. Sci. U. S. A. 14 (1928) 526–532.
[40] N.A. Dencher, D. Dresselhaus, G. Zaccai, G. Büldt, Proc. Natl. Acad. Sci. U. S. A. 86 (1989) 7876–7879.
[41] K. Edman, P. Nollert, A. Royant, H. Hassan Belrhali, E. Pebay-Peyroula, J. Hajdu, R. Richard Neutze, E.M. Landau, Nature 401 (1999) 822–826.
[42] S. Kobatake, S. Takami, H. Muto, T. Ishikawa, M. Irie, Rapid and reversible shape changes of molecular crystals on photoirradiation, Nature 446 (2007) 778–781.
[43] R. Androsch, B. Wunderlich, Macromolecules 34 (2001) 5950–5960.
[44] B. Kalkan, T.G. Edwards, S. Raoux, S. Sen, J. Chem. Phys. 139 (2013), 084507-1-084507-5.
[45] K. Bhattacharya, S. Sergio Conti, G. Zanzotto, J. Zimmer, Nature 428 (2004) 55–59.
[46] K. Das, S. Kundu, Colloids Surf. A: Physicochem. Eng. Asp. 492 (2016) 54–61.
[47] I. Horcas, R. Fernández, J.M. Gómez-Rodríguez, J. Colchero, J. Gómez-Herrero, A.M. Baro, Rev. Sci. Instrum. 78 (2007), 013705-1-013705-8.
[48] L.G. Parratt, Phys. Rev. 95 (1954) 359–369.
[49] J. Daillant, A. Gibaud, X-ray and Neutron Reflectivity: Principles and Applications, Springer, Berlin, 1999.
[50] M. Tolan, Reflectivity of x-rays from Surfaces, Springer, Berlin, 1999.
[51] J.K. Basu, M.K. Sanyal, Phys. Rep. 363 (2002) 1–84.
[52] S. Kundu, A. Datta, M.K. Sanyal, J. Daillant, D. Luzet, C. Blot, B. Struth, Phys. Rev. E 73 (2006), 061602-1-061602-6.
[53] S. Kundu, A. Datta, S. Hazra, Langmuir 21 (2005) 5894–5900.
[54] W.R. Glomm, M.H.G. Ese, S. Volden, C. Pitois, A. Hult, J. Colloid Surf. A: Physicochem. Eng. Asp. 299 (2007) 186–197.
[55] Q. He, J.B. Li, Adv. Colloid Interface Sci. 131 (2007) 91–98.
[56] G. Sui, M. Micic, Q. Huo, R.M. Leblanc, Colloid Surf. A: Physicochem. Eng. Asp. 171 (2000) 185–197.
[57] O. Brandal, T. Viitala, J.J. Sjoblom, Dispersion Sci. Technol. 28 (2007) 95–106.
[58] V.M. Bolaños-García, J. Mas-Oliva, S. Ramos, R. Castillo, J. Phys. Chem. B 103 (1999) 6236–6242.
[59] V.M. Bolaños-García, S. Ramos, R. Castillo, J. Xicohtencatl-Cortes, J. Mas-Oliva, J. Phys. Chem. B 105 (2001) 5757–5765.